Liquid - liquid doping mechanism, fabrication, numerical simulation of W - Zr(Y)O_2 alloys with excellent properties

Fangnao Xiao [a, b, c], **Thierry Barriere** [a], **Gang Cheng** [b], **Qiang Miao** [c]

[a.] FEMTO-ST Institute, CNRS/UFC/ENSMM/UTBM, Department of Applied Mechanics, Besançon, France

[b.] INSA Centre Val de Loire, Univ. Tours, Univ. Orléans, LaMé, Blois, France

[c.] College of Material Science and Technology, Nanjing University of Aeronautics and Astronautics, Nanjing, China

E-mail: fangnao.xiao@femto-st.fr

Outline

- **Introduction**
- **Liquid-liquid doping mechanism**
- **Microstructure and property of alloys**
- **Numerical modelling of particle strengthening W alloy**
- **Conclusions and perspectives**

1. Introduction

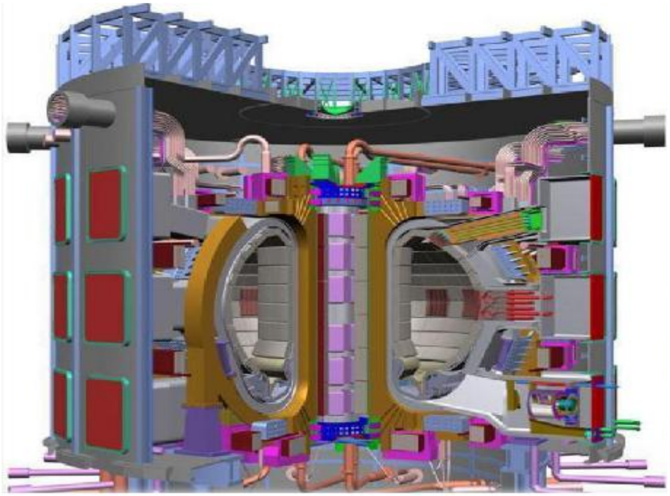

Tokamak magnetic constraints ITER system

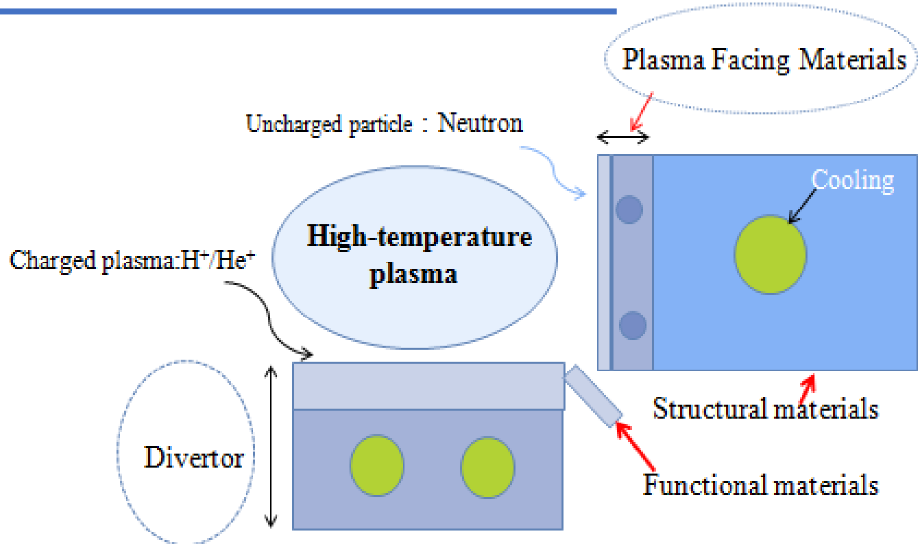

Plasma acts on the first wall and the strainer

Basic conditions as first wall W materials :

W alloys are the main high-Z candidate for strainers and the first wall plasma materials in Tokamak:

- thermal conductivity;
- high melting point;
- high toughness at low temperature;
- high stability and strength at high temperature.

Actual limitations of current W alloys fabricated by solid-solid or solid-liquid doping

Pure W: Larger initial grain size, low-temperature and high recrystallization embrittlement;

Oxide particle (La_2O_3, Y_2O_3, ThO_2) strengthening W alloy:

La_2O_3/Y_2O_3 will aggregate above 1700 ℃, resulting in the low thermodynamic stability; ThO_2 has radioactive potential.

Ti, V, Ta, Re microalloying W alloys:

The supergrains prepared by alloying are metastable, and these fine grain structures are easy to recrystallization at high temperature;

Carbon particles strengthening W alloy:

Uneven particle distribution, larger oxide particles, introducing impurities by ball-milling process and then reducing the boundary strength.

Objectives by innovative liquid-liquid doping

1. Nanosized oxide particles (< 500 nm) uniformly distributed within W grains;
2. Lower ductile-brittle transition temperature and higher recrystallization temperature (> 1400 ℃).
3. Theoretical approaches for the numerical modelling of particle strengthened W alloy

2. Mechanism of liquid-liquid doping processes

Existing forms and reaction mechanisms of polytungstate ions [1]

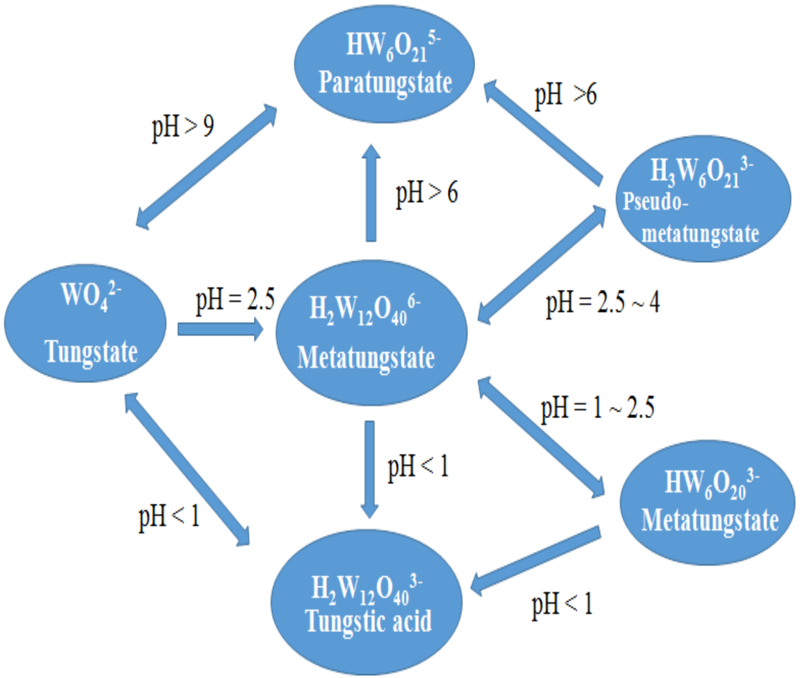

Reversible reaction equations	Reaction products	Common names
$(H_2W_{12}O_{40})^{6-}+6H^{+}+32H_2O=12(H_2WO_4\cdot 2H_2O)$	$H_2WO_4\cdot 2H_2O$	Tungstic acid
$H_2W_{12}O_{40}^{6-}+H^{+}=HW_{12}O_{39}^{5-}+H_2O$	$H_2W_{12}O_{40}^{6-}$ $/HW_{12}O_{39}^{5-}$	Metatungstate
$HW_{12}O_{39}^{5-}+2H_2O+OH^{-}=2(H_3W_6O_{21})^{3-}$	$(H_3W_6O_{21})^{3-}$	Pseudo-AMT
$(H_3W_6O_{21})^{3-}+2OH^{-}=(HW_6O_{21})^{5-}+2H_2O$	$(HW_6O_{21})^{5-}$	Paratungstate
$(HW_6O_{21})^{5-}+3H_2O+7OH^{-}=6(HWO_4)^{-}+H^{+}+7OH^{-}=6WO_4^{2-}+7H^{+}+7OH^{-}$	WO_4^{2-}	Tungstate ion

[1] F. N. Xiao, J. Alloy Compd. 774 (2019) 210–221

Liquid-liquid doping techniques for preparing $Zr(Y)O_2$ doped W powders

Hydrothermal method

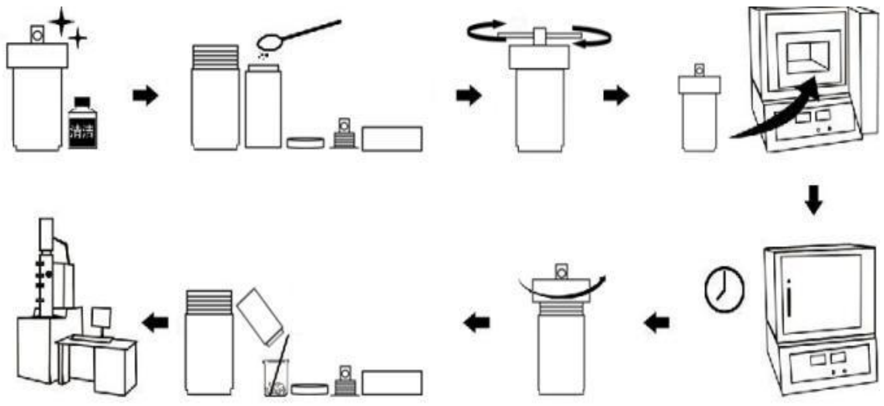

Hydrothermal reaction: 170 ℃

Duration: 12 hours

Azeotropic distillation method

Bath Temp.: 100 ℃

Dispersant: Alcohol + n-butyl alcohol

Sol-gel method

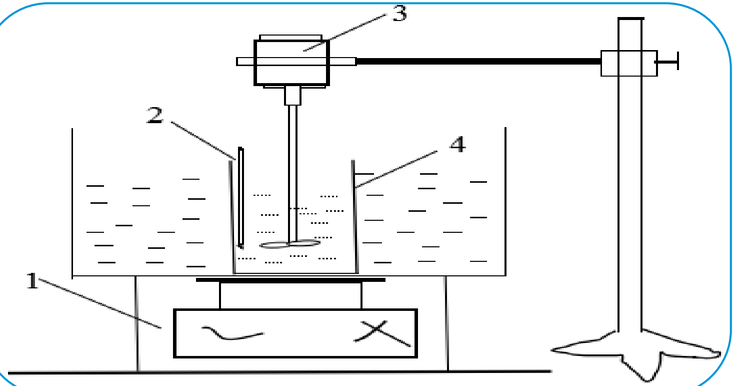

1 - Water bath
2 - Thermometer
3 - Digital stirring
4 - Beaker

Morphologies of precursors synthesized by three doping processes

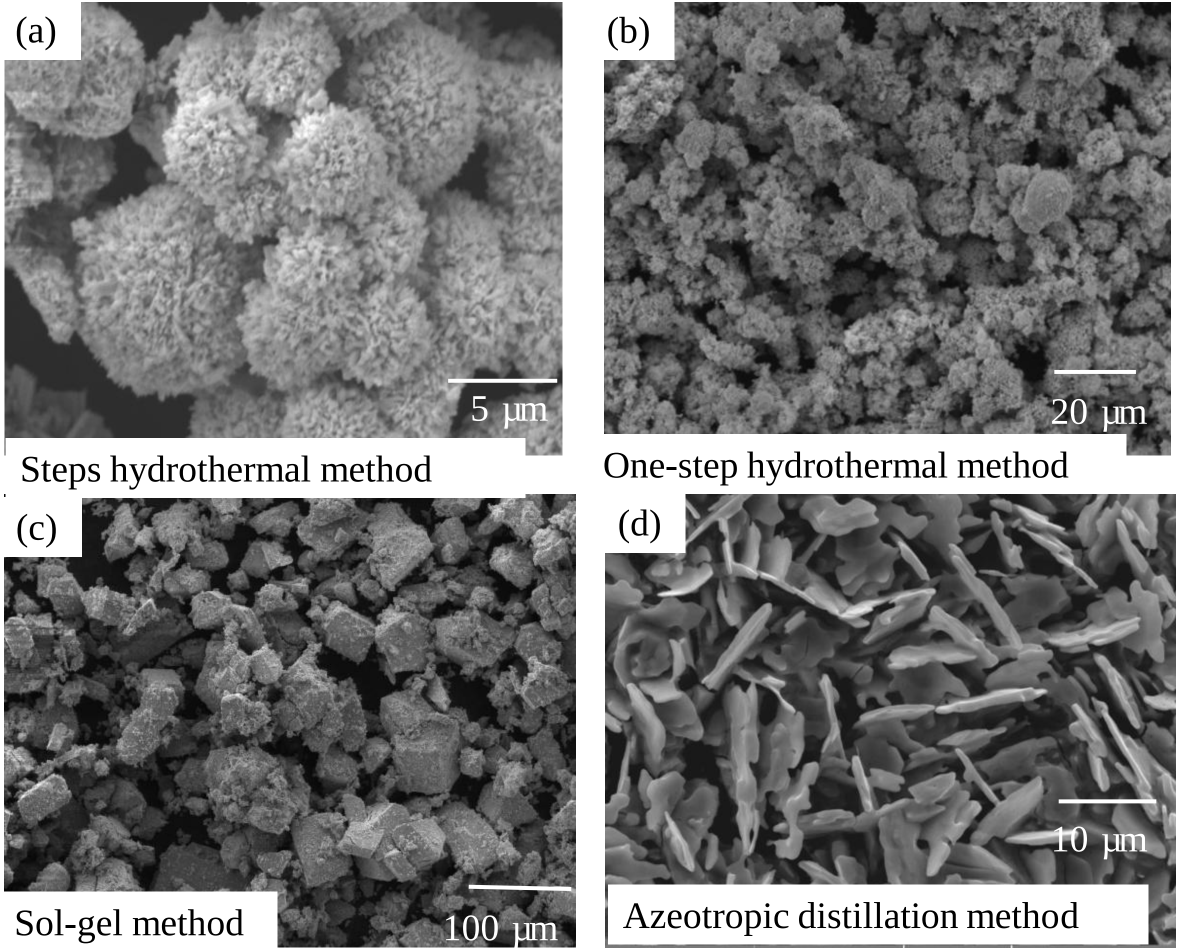

Precursors’ morphologies:

(a) Microsphere;
(b) Loose;
(c) Angularity;
(d) Sheet.

Formation mechanism of doped precursor powders

1. Synthetization analysis of h-HATB powder by hydrothermal method

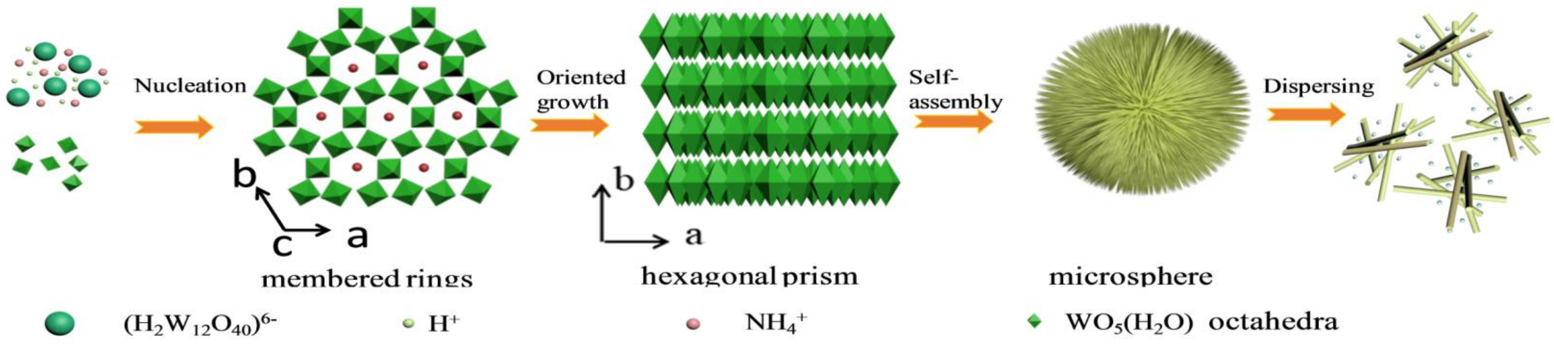

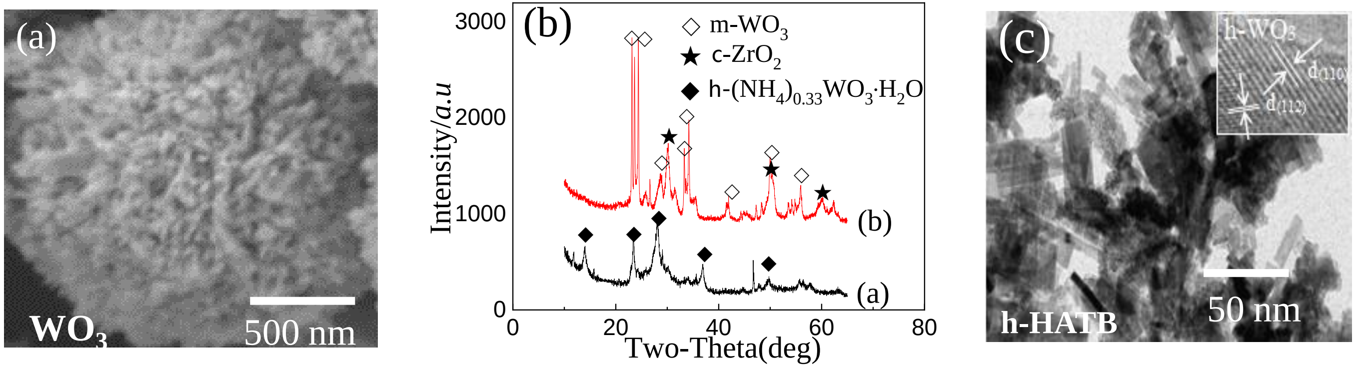

Experimental observation of the synthetization of h-HATB

F. N. Xiao et al., J Alloy Compd. 843 (2020) 156059

Formation mechanism of doped precursor powders

2. Synthetization analysis of precursor powder by azeotropic method

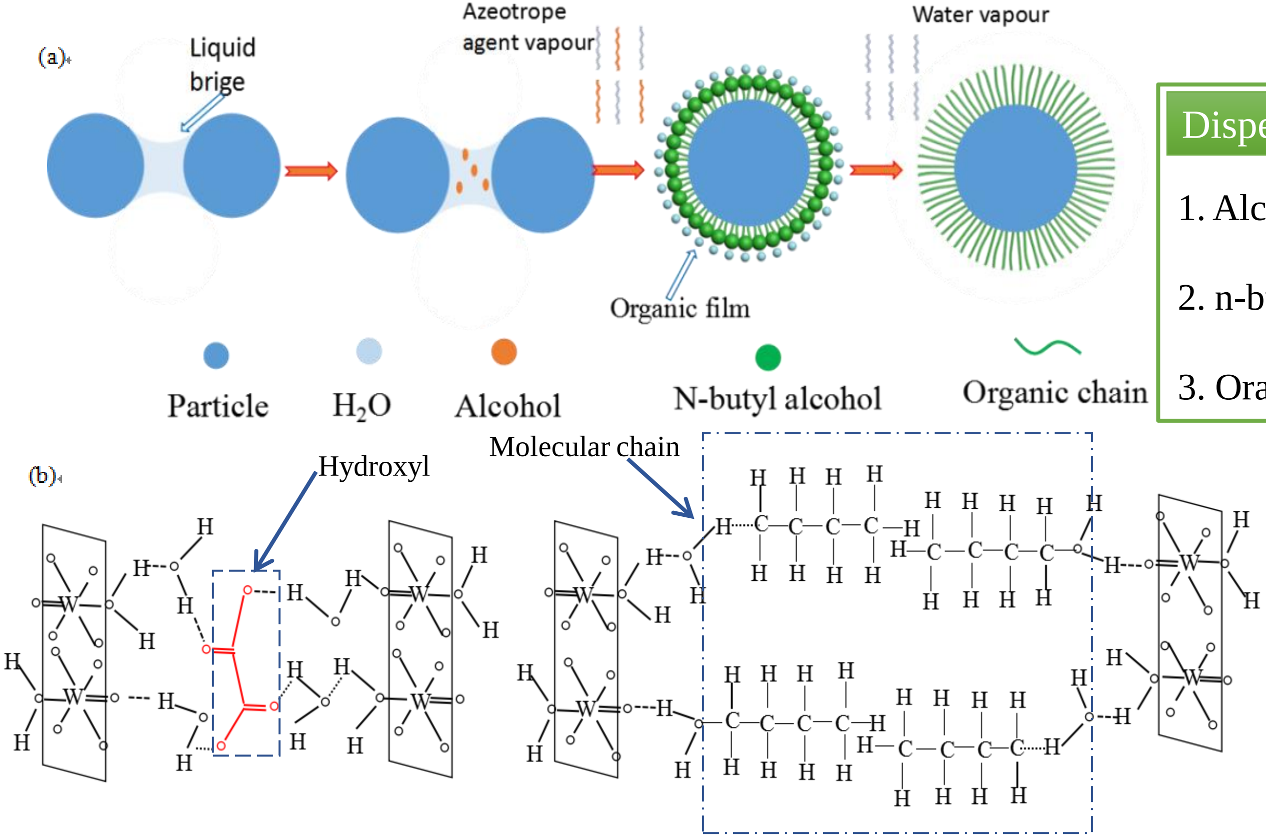

Dispersing process

1. Alcohol removing water;
2. n-bulty covering particles;
3. Oranic chain replacing hydroxly.

F. N. Xiao et al., J Alloy Compd. 855(2021) 157335

Morphologies of W- $Zr(Y)O_2$ powders reduced at 900 ℃ for 2 h

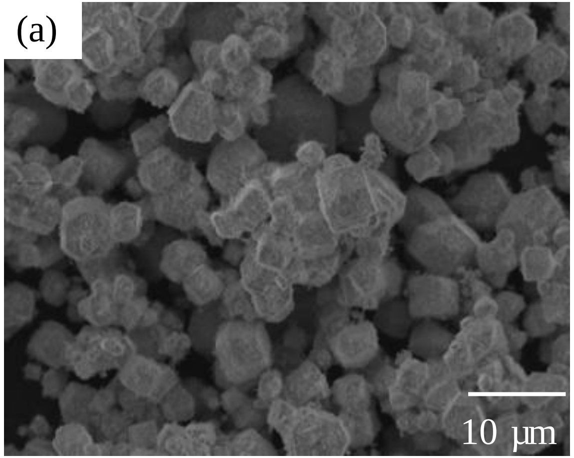

StepS hydrothermal

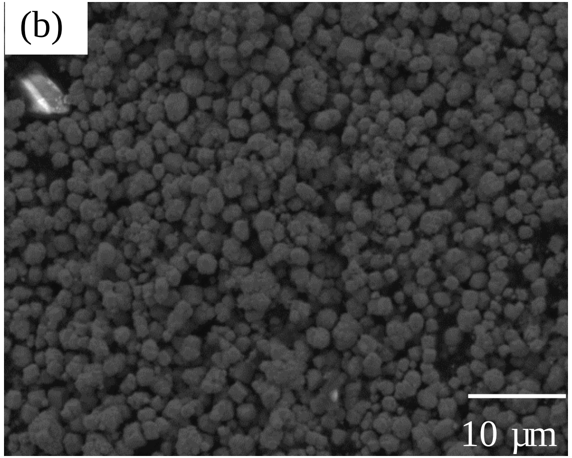

One-step hydrothermal method

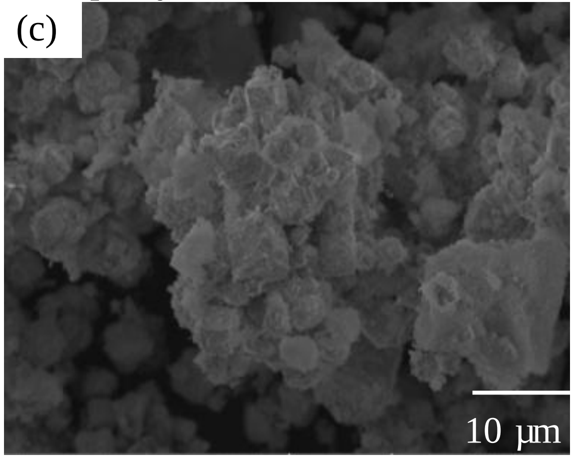

Sol-gel method

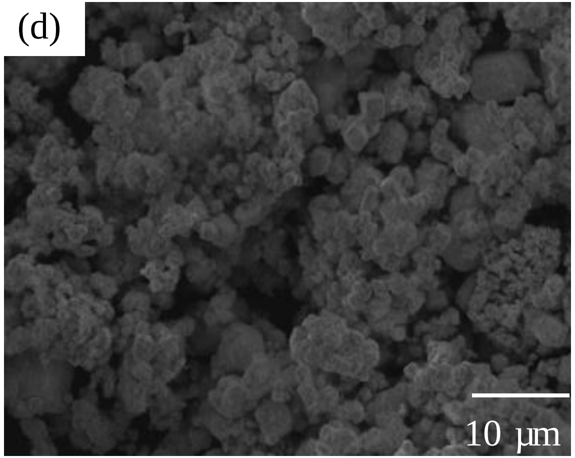

Azeotropic distillation method

1. Preserving the precursor morphologies;
2. More uniformed – size and highly dispersed powders in Fig. b

F. N. Xiao et al., J Alloy Compd. 855(2021) 157335

3. Microstructure and properties of Z(Y)O_2 strengthened W alloy

Description of innovative liquid – liquid doping process with optimal parameters

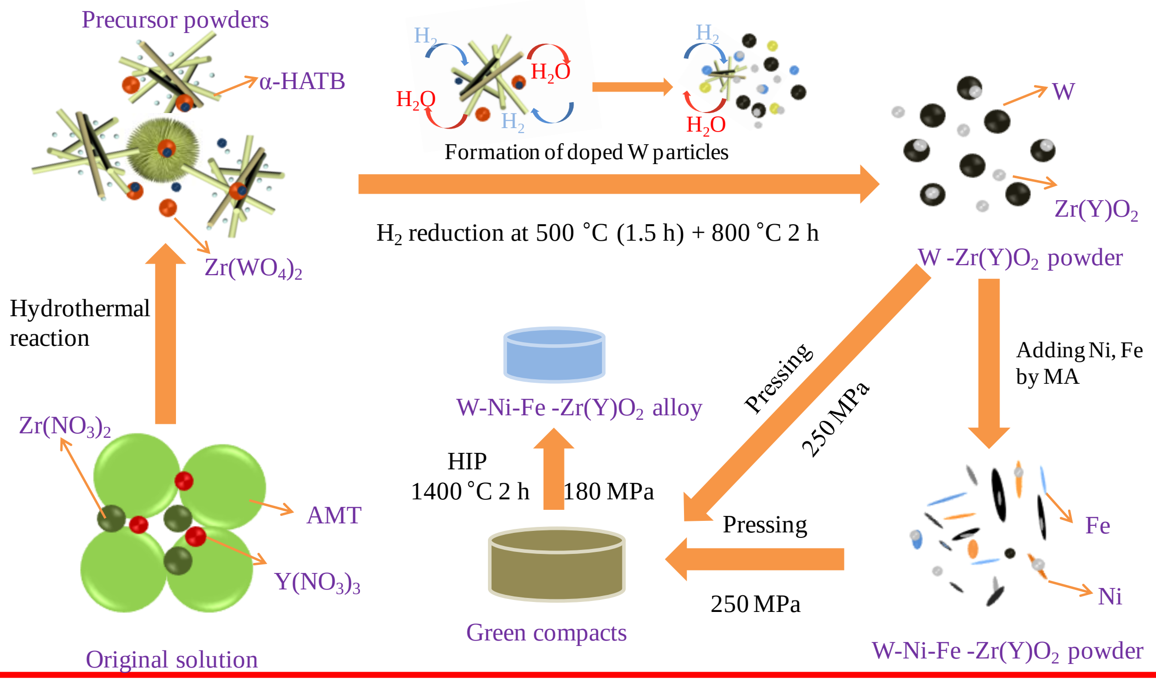

Ionic reaction mechanisms:

1. $2Zr^{4+} + W_{12}O_{40}^{8-} = 8WO_3\downarrow + 2Zr(WO_4)_2\downarrow$

2. $(H_2W_{12}O_{40})^{6-} + 6H^+ + 32H_2O = 12(H_2WO_4 \cdot 2H_2O)$

Microstructure of the advanced material

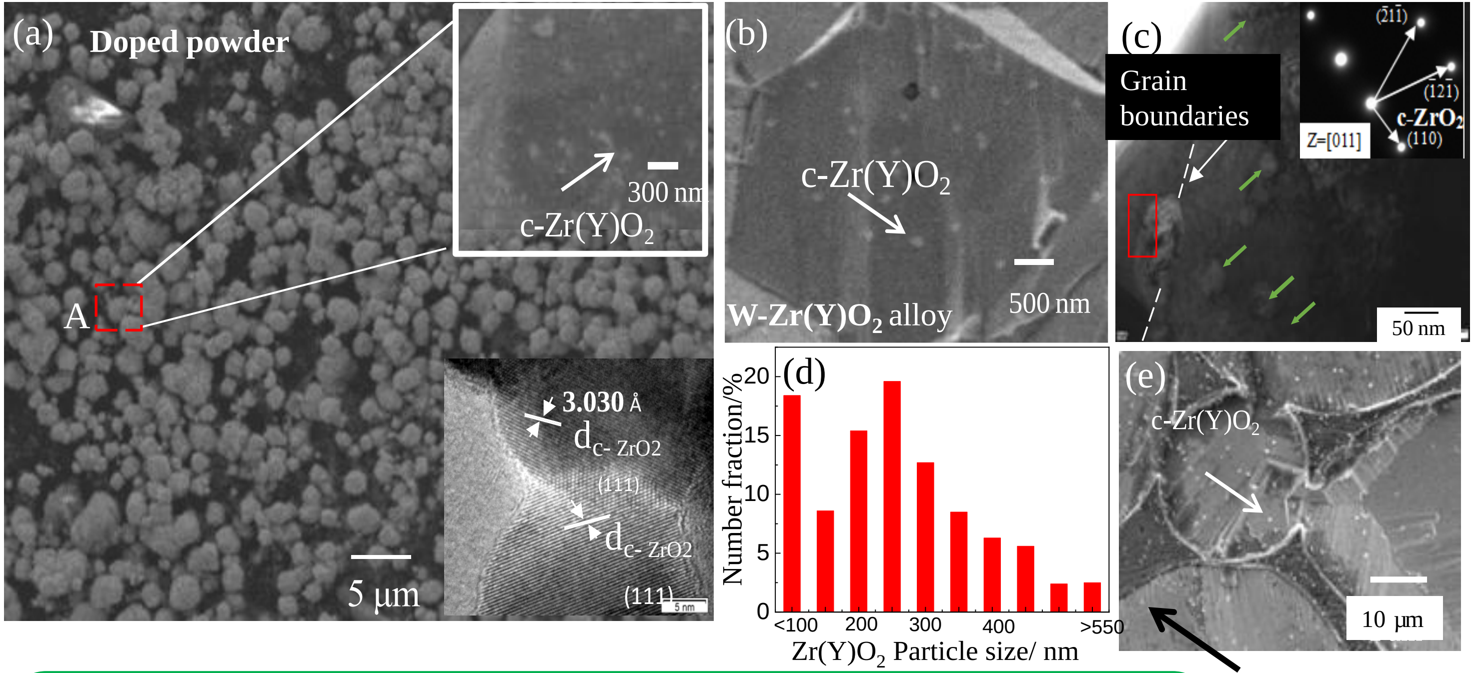

W-Ni-Fe-Zr(Y)O_2 alloy

Microstructure characterization

1. Highly dispersed doped powders, shown in Fig. (a);
2. 90% of particles distributed within W grains, shown in Fig. (b) and (e);
3. 85% of Zr(Y)O_2 particles are less than 300 nm in size, shown in Fig. (d).

F. N. Xiao et al., J. Alloy Compd. 774 (2019) 210–221

Comparison with state-of-the-art review

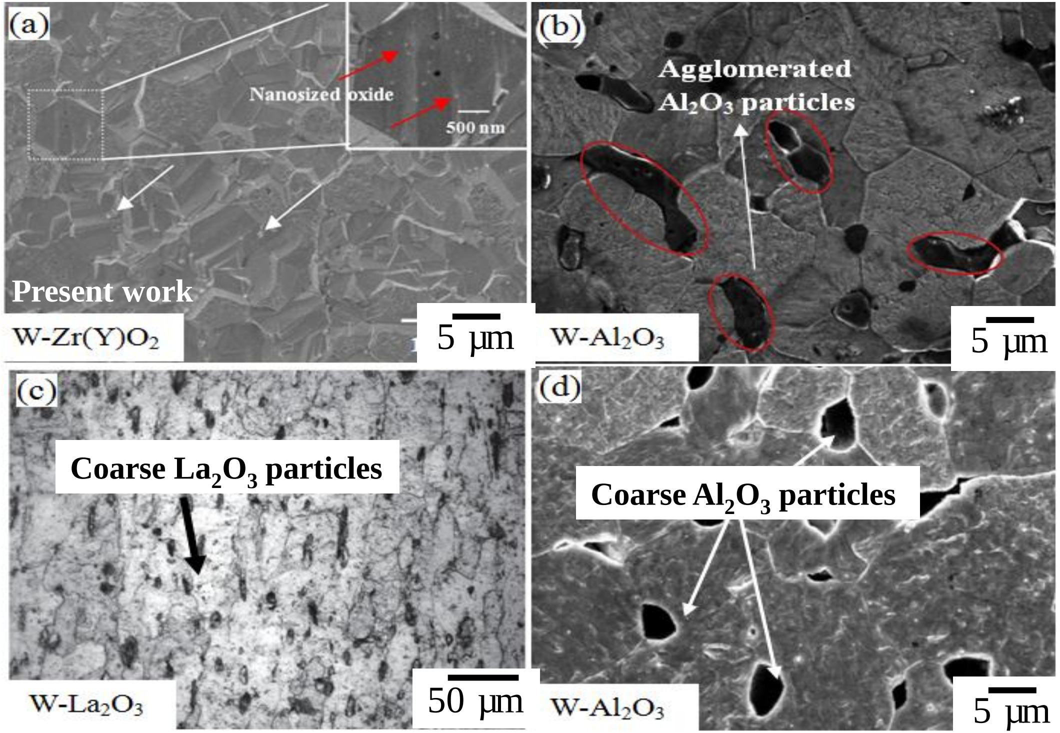

References

(a) Present work;
(b) C. J. Wang, J. Refract. Met. Hard Mater. 84 (2020) 105082;
(c) Y. Shen, J. Nucl. Mater. 455 (2014) 234-241;
(d) M. A. Yar, J. Nucl. Mater. 412 (2011) 227-232.

Main characteristic of the advanced W alloys

1. The oxide particle are smallest;
2. More oxide particles distributed within W grains;
3. The distribution of oxide particles are more uniform.

Comparison of microstructure and properties of ODS-W alloys

Doping process	Sintering Process	Alloy	W grain size	Oxide size	Relative density	Microhardness	Refs.
	SPS	W-6vol% l_2O_3	3.64 μm	>1.0 μm	94.96 %	347.39 HV	[35]
L - L	SPS	W-2.5%ZrO_2	4.65 μm	2.5 μm	99.6 %	480 HV	[36]
	VD	W-2.5%ZrO_2	40-80 μm	1.5μm	98.7 %	-	[37]
	VD	W-La_2O_3	50 μm	3 μm	-	-	[38]
L - S[a*]	SPS	W-0.9wt%La_2O_3	-	2 μm	94 %	406 HV	[39]
	SPS	W-1.0%Y_2O_3	2.3 μm	Nanosize (Uneven)	92 %	423 HV	[40]
	HIP	W-1%La_2O_3	-	>5 μm	90.6 %	-	[41]
S - S	HIP	W-Ti-0.5%Y_2O_3	2-5 μm	>1.5 μm	-	-	[42]
	SPS	W-5%HfO_2	11.6 μm	>5 μm	94.5 %	440	[43]
Novel process	**HIP**	**W-0.5%Zr(Y)O_2**	**4.67±0.5 μm**	**0.25 ± 0.05 μm**	**96.7 ± 0.2 %**	**472 ± 10 HV**	**Present**

Conclusion

1. Smallest particles size; 2. Medium properties.

F. N. Xiao et al., J Alloy Compd. 843 (2020) 156059

Comparison with state-of-the-art review

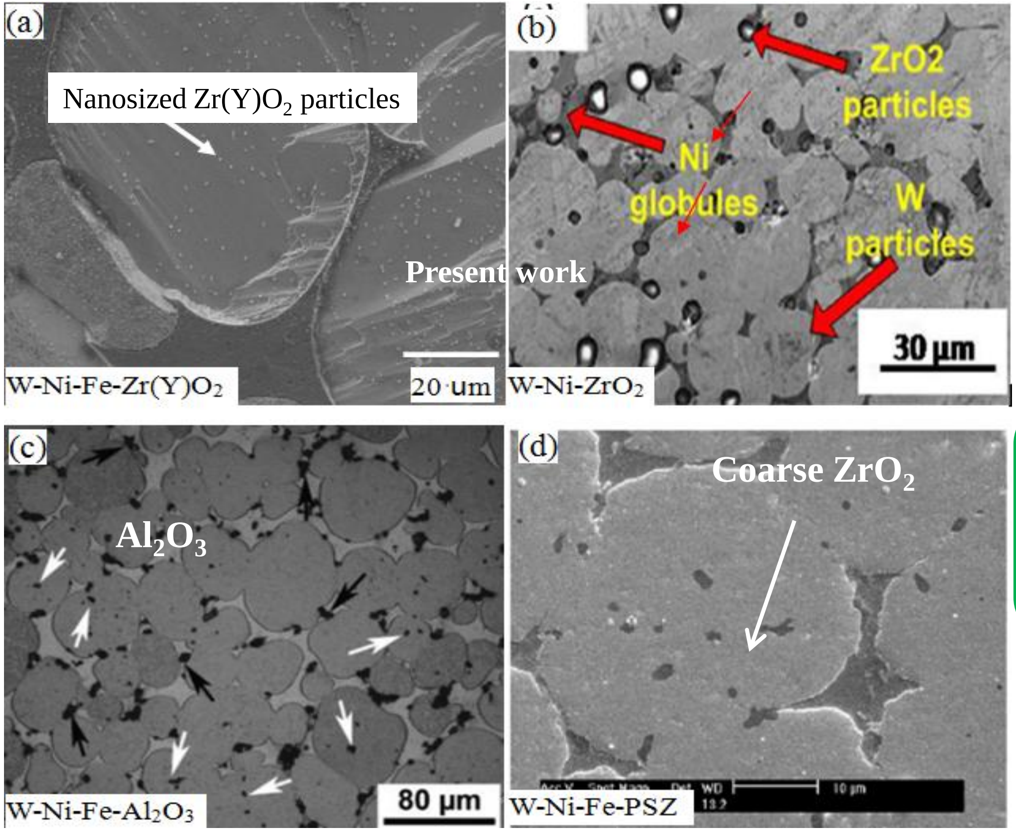

References

(a) Present work;
(b) W. M.R. Daoush Mater. Sci. Eng. A. 2016, 47(5): 2387-2395;
(c) K. H. Lee, J. Alloy. Compd. 2007, 434: 433-436;
(d) K. Hu, Mater. Sci. Eng. A. 2015, 636: 452-458.

Main characteristic of my prepared heavy W alloy

1. The oxide particle are smaller;
2. Most $Zr(Y)O_2$ distributed within W grains;
3. The distribution of oxide particles are more uniform.

Comparison of microstructure and properties of ODS-heavy W alloys

Heavy W alloy	Sintering process	RD	Grain size	Particle size	Hardness	Refs.
W–Ni-Fe–0.3PSZ	1480 ° C (1h)	-	18 μm	0.8 μm	-	[49]
W–Ni-Fe-1Al_2O_3		98.3 %	36.8 μm	7 μm	-	[52]
W–Ni-Fe–xY_2O_3	1485° C (1h)	99.1 %	19.5 μm	0.6 - 1.3 μm	-	[10]
W-Ni-ZrO_2	1500° C (1h)	93.5 %	~25 μm	3 – 5 μm	333 HV	[50]
W-Ni-Fe-Co-Y_2O_3	1450° C (1h)	94.1 %	12 μm	>0.6 μm	425 HV	[44]
94W-4.56Ni-1.14Fe-Y_2O_3	1485° C (1h)	99.0 %	15 μm	0.65 μm	-	[53]
Previous W-ODS	SPS/HIP	<99.9 %	<10 μm	1 – 5 μm	406 – 480 HV	[27]
93W-4.9Ni-2.1Fe-Zr(Y)O_2	1520° C (2.5h)	99.2 %	26 μm	0.2 – 1 μm	402 HV	[47]
$WHA_{0.75}$	**1400° C (2.5h)**	**99.2 ± 0.1 %**	**25 ± 2 μm**	**0.2 – 1 μm**	**402 ± 10 HV**	**Present**

Conclusion

1. Finer particles;
2. Larger grain size;
3. Limited grain refinement.

F. N. Xiao et al., J Alloy Compd. 2020, 843: 156059

TEM analysis of HIP sintered W-Ni-Fe-ZrO_2 alloys

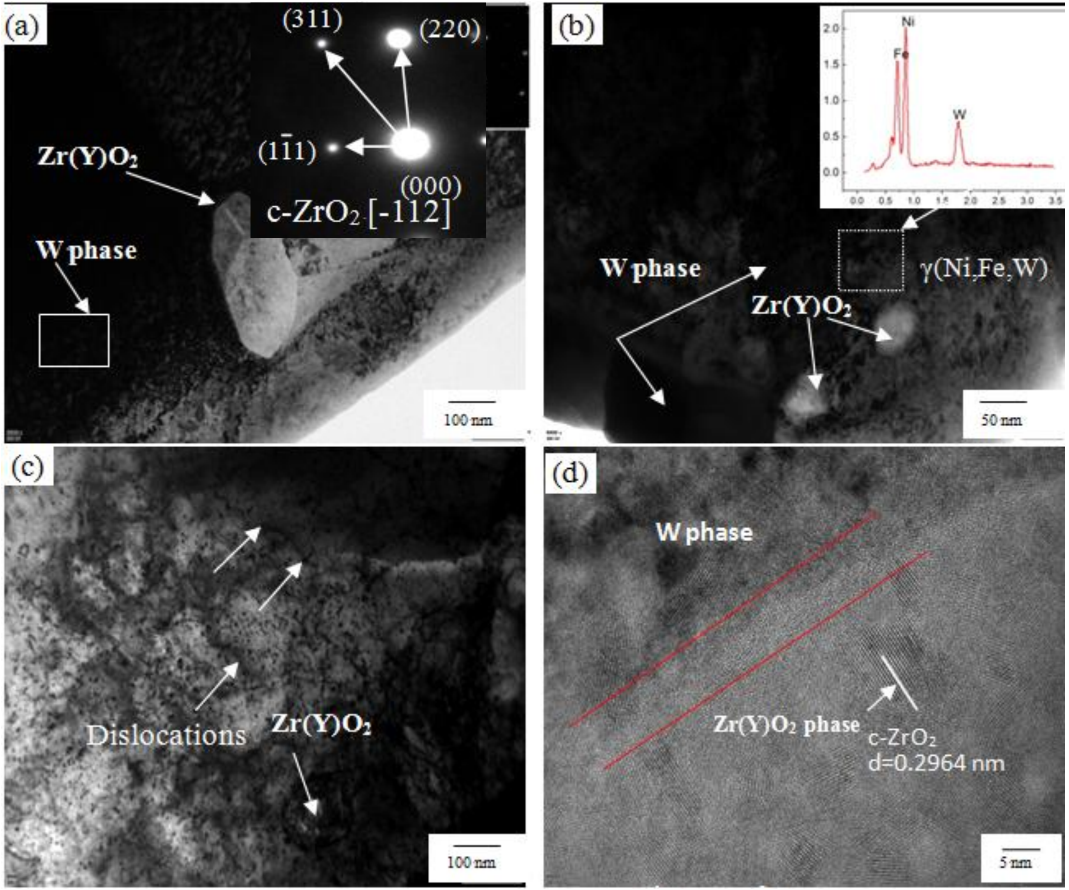

Conclusion

1. Cubic structure of Zr(Y)O_2;
2. Well - bonded interface.

Comparison of mechanical properties with state-of-the-art review

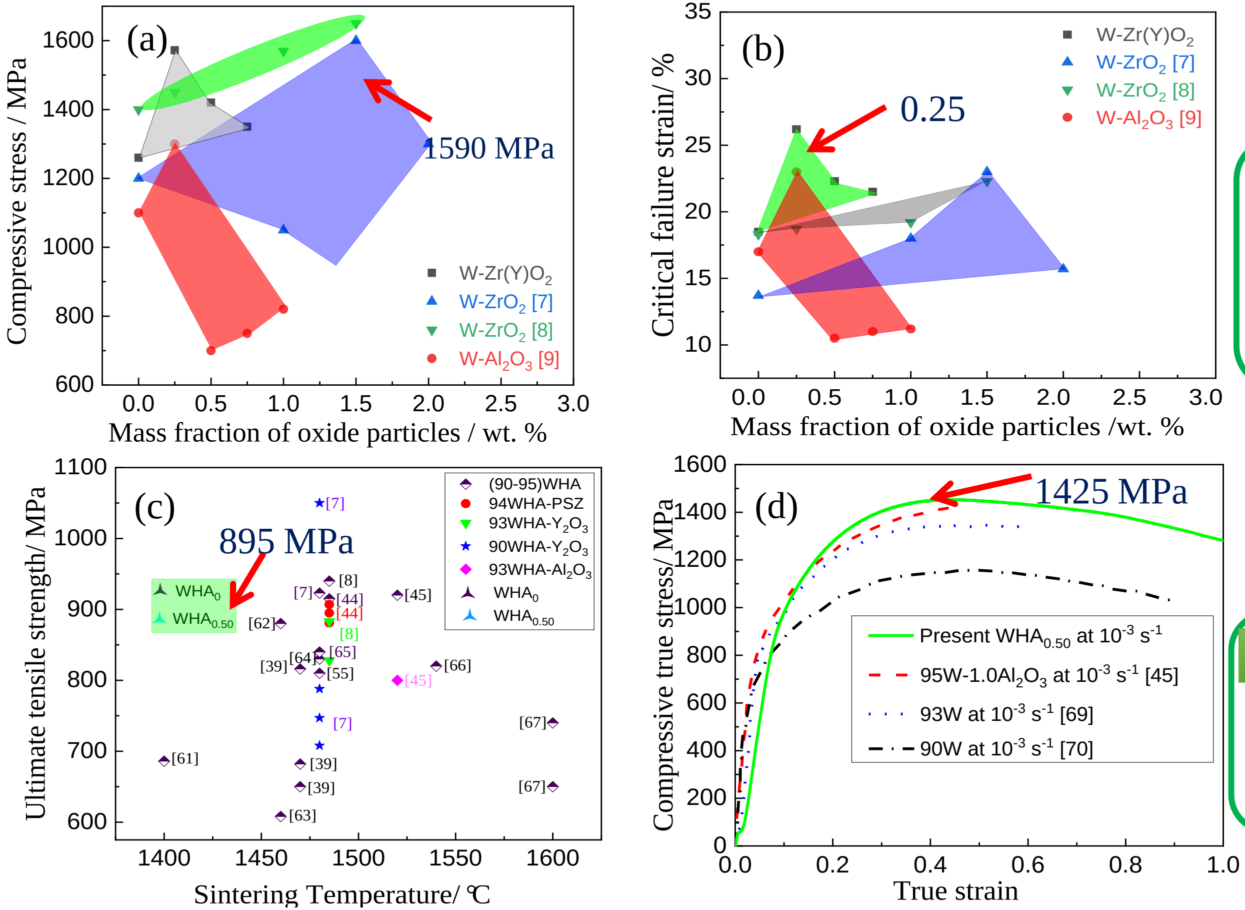

W-Zr(Y)O$_2$ alloy in fig (a, b)

1. High compressive strength;
2. High critical failure strain;
3. Higher than published alloys.

93W-Zr(Y)O$_2$ alloy in fig (c, d)

1. Higher tensile strength;
2. Compressive strength.

F. N. Xiao et al., J Alloy Compd. 2020, 824:153894

Mechanical properties of $W\text{-}Zr(Y)O_2$ alloy at high temperatures

Objective: Arrhenius model was used to identify the compressive behaviours of the $W\text{-}Zr(Y)O_2$ alloy.

$$Z = A\,[\sinh(\alpha\sigma)]^n$$

$$\downarrow$$

$$\ln Z = \ln A + n \ln [\sinh(\alpha\sigma)]$$

$$\downarrow$$

$$\ln \dot{\varepsilon} = \ln A + n \ln [\sinh(\alpha\sigma)]$$

$$\text{AARE} = \frac{1}{N}\sum_i^N \left|\frac{(\sigma_e{}^i - \sigma_p{}^i)}{\sigma_e{}^i}\right| \times 100\%$$

$$\alpha = A_0 + A_1\varepsilon + A_2\varepsilon^2 + A_3\varepsilon^3 + A_4\varepsilon^4 + A_5\varepsilon^5 + A_6\varepsilon^6$$

$$n = B_0 + B_1\varepsilon + B_2\varepsilon^2 + B_3\varepsilon^3 + B_4\varepsilon^4 + B_5\varepsilon^5 + B_6\varepsilon^6$$

$$\ln Z = C_0 + C_1\varepsilon + C_2\varepsilon^2 + C_3\varepsilon^3 + C_4\varepsilon^4 + C_5\varepsilon^5 + C_6\varepsilon^6$$

Z is Zener-Hollomon parameter;

ε is strain;

$\dot{\varepsilon}$ is strain rate;

A, n and α are material constants.

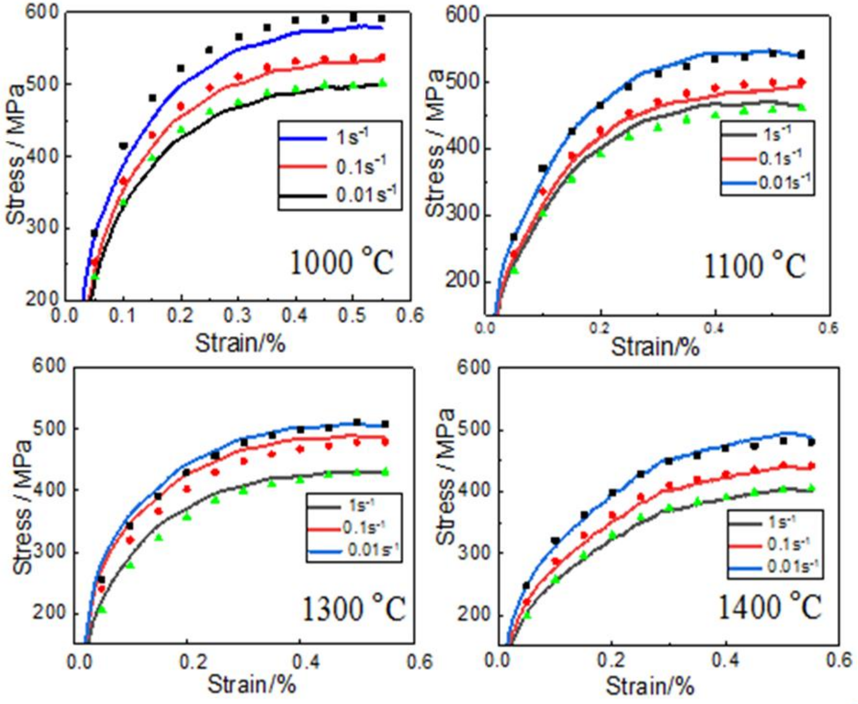

Conclusion: The average relative error (AARE) = 3.6 % was calculated to investigate the high prediction accuracy.

4. Numerical modelling of $Zr(Y)O_2$ particle strengthening W alloy

Methodology of numerical approach based on the compressive tests

Equivalent homogeneous distribution of particle–matrix interactions

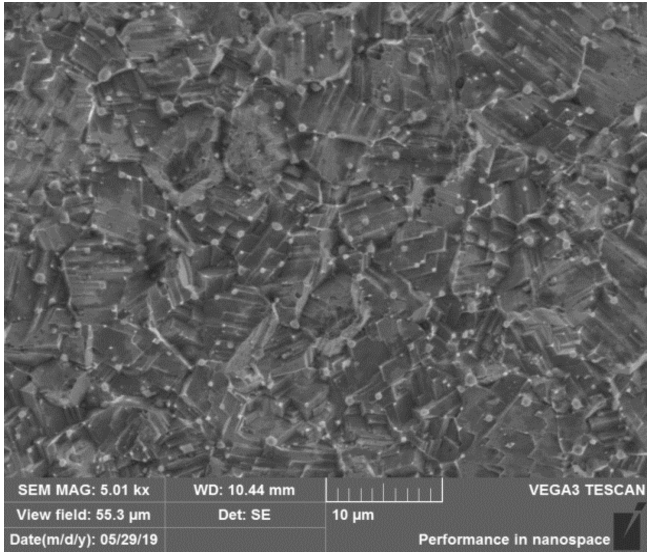

Microstructure of the reference material (SEM observation).

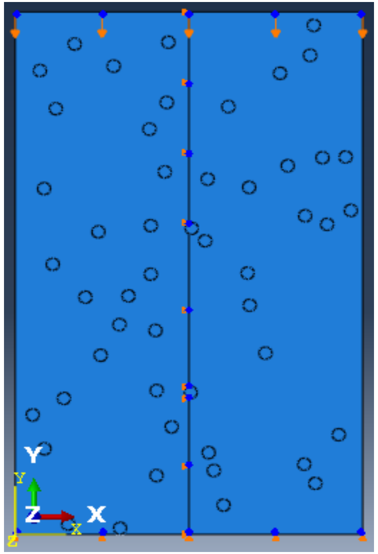

Generated simulation model with equivalent representative elementary volume (REV)

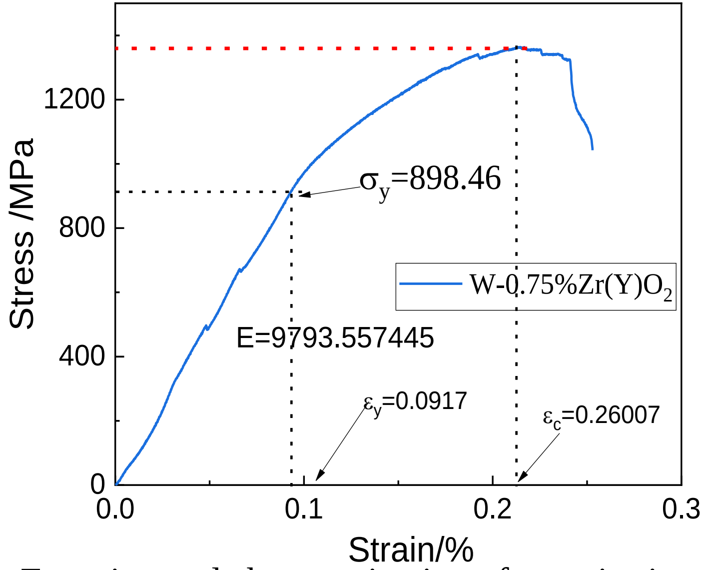

Experimental characterization of constitutive behaviour of the particle strengthening W alloy

Sample size: 5 x 8 mm

F. N. Xiao et al., J Alloy Compd. 2020, 843: 156059

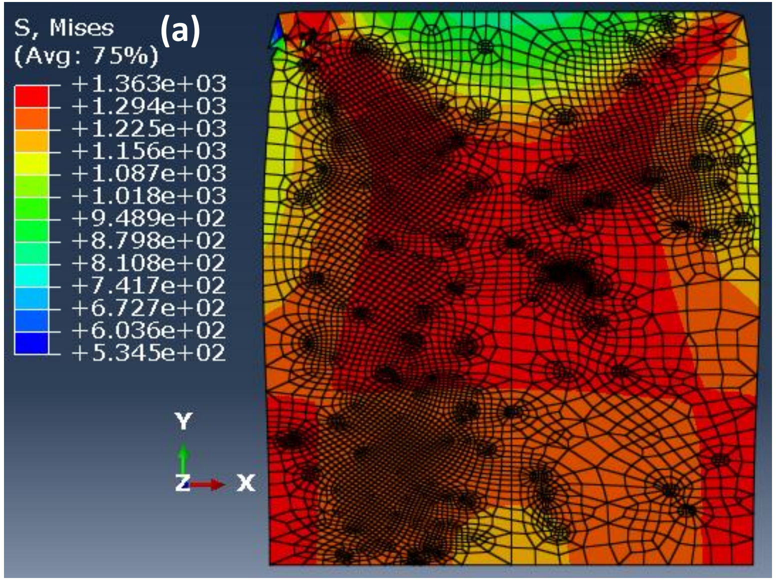

Particle strengthening model

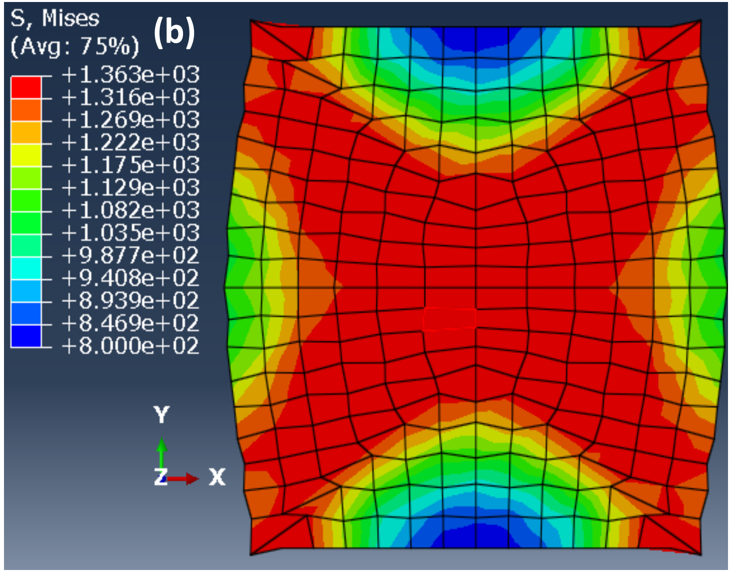

No particle strengthening model as reference

Conclusion:

With the particle, the stress distribution are complicated;
Without particles, the distribution are symmetrical.

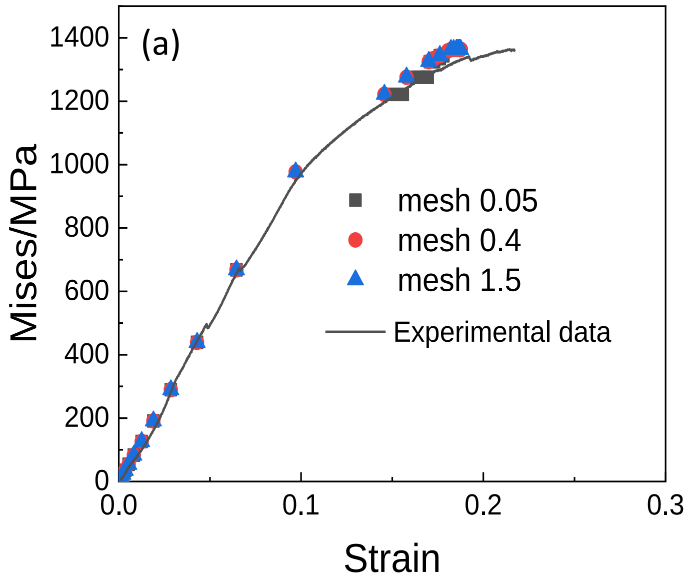

Mises stress vs strain from 50 particle strengthening model

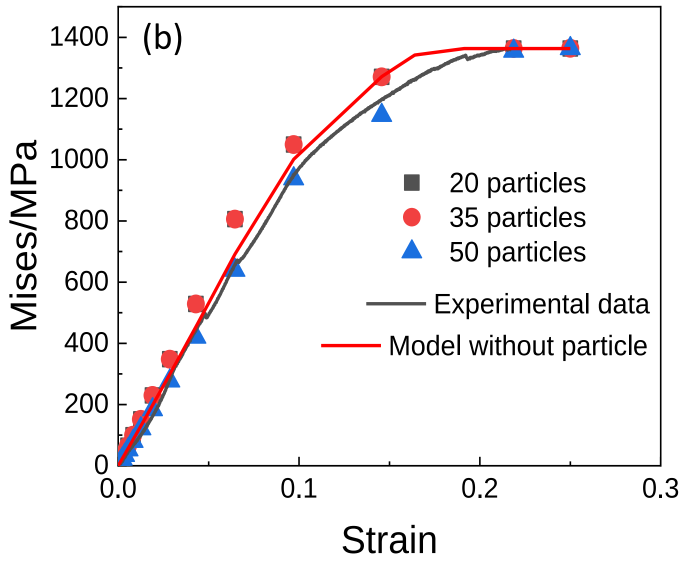

Mises stress vs strain obtained from model with 0.4 mesh size

Conclusion:

1. Slight influence of mesh size;
2. High accuracy from particle strengthening model;
3. Higher prediction ability with smaller particles.

Conclusions

1. Investigation of reaction mechanism and formation mechanism of doped W precursor powders;
2. Development of an innovative liquid – liquid hydrothermal doping process;
3. Fabrication of W alloys having ZrO_2 particles (< 300 nm) within grains;
4. Fabrication of advanced W alloys with high strength and critical failure strain;
5. Numerical simulation with particle reinforced model.

Perspectives

1. Experimental characterization in tensile and bending tests at various temperatures (100 ~ 1500 ℃);
2. Micro- and nano- scale numerical simulation with equivalent representative elementary volume ;
3. Extension of the developed method for Y_2O_3, La_2O_3 and CeO_2 strengthened W alloy.
4. Future application of these reinforced innovative material for different powder forming processing.

Thank you for your attention!